Arabian Journal for Science and Engineering (2024) 49:637–647
https://doi.org/10.1007/s13369-023-08267-w

RESEARCH ARTICLE-CHEMISTRY

Synthesis and Applications of Crown Ether-Linked Metal–Organic Framework Composite-Based Sensors for Stripping Voltammetric Determination of Lead

Rehab O. El-Attar[1] · Reda M. Abdelhameed[2] · Elmorsy Khaled[1]

Received: 25 March 2023 / Accepted: 22 August 2023 / Published online: 16 October 2023

Abstract
The present work demonstrates the construction and electrochemical characterization of novel disposable screen-printed carbon sensors integrated with functionalized MIL-53-NH_2 metal–organic framework cross-linked with crown ethers and calixarene macrocyclic compounds for sensitive differential pulse voltammetric determination of lead ions in tap, surface water and biological fluid samples. The electroanalytical parameters were optimized regarding the nature of the electrode modifier, supporting electrolyte, the working pH value, scan rate, deposition potential, deposition time, reproducibility of measurement and the operational lifetime. Working electrodes dropcasted with MIL-53-NH_2-dibenzo-24-crown-8-ether nanocomposite (MOFCE24) showed the proper performance within the lead concentration ranging from 13.75 to 217.83 ppb with LOD and LOQ values of 3.18 and 9.62 ppb, respectively. The synergistic effect of the metal–organic frameworks as transducer and dibenzo 24-crown-8-ether as sensing elements accelerates the electron transfer process at the electrode surface and improves the sensor selectivity through complexation of the lead ions with the crown ether moiety. The fabricated sensors showed high measuring reproducibility with long operational life time (60 days), which can be attributed to the formation of cross-linked ionophore/metal–organic framework with limited leaching of the sensing element in the measuring solution. The introduced sensors were utilized for the onsite voltammetric determination of lead in environmental and biological samples with acceptable average recoveries comparable with the graphite furnace atomic absorption spectrometric method.

Keywords Metal–organic frameworks · Cross-linked macromolecules · Screen-printed voltammetric sensors · Lead · Environmental and biological samples

1 Introduction

Contamination with toxic heavy metals represents one of the most significant environmental pollutants and comes second to pesticides [1–3]. Heavy metals are a threat to the environment as they are not biodegradable; therefore, they are retained indefinitely in the ecological systems and food chain [4]. Among them, lead ions with their high toxicity are serious contaminants with extreme toxicity to the environment and human health, even at low concentration levels [5]. Contamination of the drinking water with lead ions causes many severe health problems such as convulsions, coma, cancer, nausea, renal failure and severe effects on the metabolism and intelligence [6, 7]. Therefore, contentious onsite monitoring of lead even at trace levels in the environmental and food samples is of utmost concern for public health. Atomic absorption spectrometry and atomic emission spectrometry with inductively coupled plasma excitation are the most common analytical approaches for monitoring heavy metal ions [8].

Electroanalytical approaches, particularly stripping voltammetric technique, can participate and complement atomic spectroscopy for monitoring of trace heavy metal residues [9–11]. More than 40 trace elements can be detected voltammetrically with high sensitivity and precision in biological and environmental samples [12, 13]. The unique coupling of the effective pre-concentration steps and

✉ Rehab O. El-Attar
rhbattar@yahoo.com

[1] Microanalysis Laboratory, Applied Organic Chemistry Department, National Research Centre, El Bohouth St., Dokki, Giza 12622, Egypt

[2] Applied Organic Chemistry Department, National Research Center, El Bohouth St., Dokki, Giza 12622, Egypt

advanced measurement procedures remarkably enhanced the sensitivity of the stripping voltammetric analysis [14–19].

Anodic stripping voltammetric determination of lead at mercury-based working electrodes was the most popular [20–22]. Meanwhile, due to restrictions for applications and handling of the most toxic mercury metal and its compounds, mercury was replaced by other metallic films for voltammetric monitoring of heavy metal residues [23–25]. Among them, the eco-friendly bismuth film behaves similar to mercury and forms fused alloys with many heavy metals.

Tailor-made electrochemical sensors integrated with selected ligands and macromolecules were reported to possess improved sensitivity and selectivity toward the target analyte [26]. Homemade disposable screen-printed sensors with printing ink fortified with chitosan showed successful simultaneous voltammetric determination of Pb, Cu, Cd and Hg ions in spiked tape water sample with high sensitivity and selectivity [27].

Metal–organic frameworks (MOFs) were introduced as new promising functional materials due to their high surface area, large pore volumes and porosity [28–32]. Moreover, MOFs can be easily functionalized with various macromolecules and metallic nanostructures with tunable properties and the synergic effect of both components. Electrochemical systems based on MOF-functionalized composites were reported as efficient sensing platforms [33–37]. Carbon paste electrodes (CPEs) integrated with MOF-5 (Zn_4O (1,4-benzenedicarboxylate)$_3$) were constructed for sensitive differential pulse stripping voltammetric determination of lead with a linear range from 1.0×10^{-8} to 1.0×10^{-6} mol L^{-1} [38]. Glassy carbon sensors modified with flake-like NH_2-MIL-53(Cr) MOF or Ni-based MOF were applied for detection of microgram levels of Pb^{2+} in aqueous solution [39, 40]. UiO-66-NH_2-graphene nanocomposites were also reported for simultaneous voltammetric detection of multiple heavy metal ions in aqueous solution [41].

For improved selectivity and sensitivity of novel electrochemical sensors, trials were executed to integrate the working electrode matrix with different carbonaceous and metallic nanostructures, which offer various advanced analysis opportunities with enhanced sensor performance [42–46]. Based on the electrocatalytic activity of the incorporated nanostructures, the electron transfer kinetics takes place at the electrode surface were enhanced with noticeable shift of the redox potential of the target analyte toward the negative direction.

The present work described the detailed synthesis, characterization and application of novel cross-linked macromolecules-metal–organic framework nanocomposites for sensitive adsorptive differential pulse voltammetric determination of lead in environmental and biological samples. The electroanalytical parameters were optimized regarding the nature of the electrode modifier, supporting electrolyte, the working pH value, scan rate, deposition potential, deposition time, reproducibility of measurement and the operational lifetime. The synergistic effect of the metal–organic frameworks as transducer within the nanocomposite and dibenzo 24-crown-8-ether (MOFCE24) as sensing elements accelerate the electron transfer process at the electrode surface and improve the sensor selectivity through complexation of the lead ions with the crown ether moiety.

2 Experimental

2.1 Chemicals and Reagents

Analytical grade reagents and ultrapure water with electric resistivity ~ 18.3 MΩ cm (Milli-Q system, Millipore) were used for the preparation of supporting electrolyte and stock solutions. Selected cyclic macromolecules were cross-linked with the synthesized functionalized metal–organic framework including 18-crown-6 ether (Fluka), dibenzo 24-crown-8 ether (Fluka) and calix[8]arene (Aldrich). Britton–Robinson (BR) and acetate buffer solutions were tested as a supporting electrolyte. BR stock buffer solution with concentration of 4×10^{-2} mol L^{-1} was prepared by dissolving 2.47 g boric acid in a mixture of 2.7 mL phosphoric acid, and 2.3 mL glacial acetic acid, and diluted to 1 L with deionized water. The desired pH value was adjusted with sodium hydroxide solution. Acetate buffer solution (2×10^{-1} mol L^{-1}) was prepared via mixing sodium acetate solution with acetic acid, where the pH was followed with a pH-meter. Other supporting electrolytes such as KCl, HCl and HNO_3 (each 2.0×10^{-1} mol L^{-1}) were prepared by dissolving the appropriate amount of analytical grade source in distilled water. Standard lead solution (10^{-3} mol L^{-1}) was prepared by dissolving the appropriate quantity of analytical grade lead nitrate salt (BDH) in 100 mL of 1% (v/v) HNO_3 solution, and the exact concentration was examined with atomic absorption spectrophotometry.

2.2 Synthesis of MIL-53-NH_2

The MIL-53-NH_2 metal–organic framework was synthesized as follows: the reaction was carried out in 40 mL Teflon-lined stainless steel bomb filled with 28 mL water containing 0.120 g (0.66 mmol) of 2-amino-benzenedicarboxylic acid. The organic linker was dissolved in water by adding 0.56 mL (0.22 mmol) of 0.4 mol NaOH solution followed by addition of 1.10 mL (0.44 mmol) of $AlCl_3.6H_2O$ solution at room temperature. For complete growth of the framework crystal, the above reaction mixture was heated at 110 °C for 24 h. After cooling, the resultant precipitate was washed with water, DMF and soaked in CH_2Cl_2 for 24 h before being dried at 80 °C.

2.3 Synthesis of MIL-53-NH_2–Crown Ether Composites

The MIL-53-NH_2–18–crown nanocomposites were prepared as follow: MIL-53-NH_2 (0.5 g) was dispersed in 100 mL ethanol containing 0.5 g of either 18-crown-6 ether or dibenzo 24-crown-8 ether, and the reaction mixture was kept in water bath sonicatior for 2 h. After centrifugation, the solid precipitates were dried under vacuum until uses.

2.4 Synthesis of MIL-53-NH_2-Calixarene Composite (MOFCalix)

Calixarene-MOF composite was synthesized by mixing 0.5 g of MIL-53-NH_2 and 0.5 g calixarene in 100 mL ethanol with continuous stirring for 2 h followed by sonication for 2 h in water bath sonicatior to assure complete dispersing of MIL-53-NH_2 into the calixarene solution. The mixture was centrifuged and washed several times with ethanol, then dried under vacuum until uses.

2.5 Lead Samples

Tap water and surface water samples (River Nile, Giza Governorate) were boiled for the removal of the residual chlorine, and the pH was adjusted to 4.0 using HNO_3.

Standard blood and urine samples (VACSERA, Dokki, Giza) were fortified with different aliquots of the standard lead solution and digested with a mixture of 5 mL nitric acid (60%), 2 mL perchloric acid (60%) followed by few drops of hydrogen peroxide solution (30%). The mixture was heated till dryness and transferred into 25 mL measuring flask with distilled water [47, 48].

The lead contents in different samples were assayed at the optimized electroanalytical conditions following standard addition method in comparison to the atomic absorption spectrophotometry.

2.6 Electrochemical Procedures

The surface of the commercial screen-printed carbon sensors (Metrohm 110 C, with 4 mm surface area of the working electrode) were modified with two successive 10 µL aliquots of the tested nanocomposite solution (2 mg mL^{-1} in DMF). After complete dryness at room temperature, the integrated sensors were preconditioned by running five successive cyclic voltammograms in the corresponding supporting electrolyte. Differential pulse voltammograms were recorded using PSTrace (3.6-PalmSens potentiostat) in the selected supporting electrolyte solution under the following optimized electroanalytical parameters: deposition time 300 s, deposition potential − 0.9 V, pulse amplitude 0.050 V, pulse width 100 ms with pulse duration 20 ms, scan rate 0.050 Vs^{-1} and voltage step 0.01 V. The recorded peak heights (based on the baseline subtraction) were plotted against the corresponding lead concentration. All experiments were performed at room temperature under atmospheric conditions.

3 Results and Discussion

3.1 Characterization of Metal–Organic Frameworks Cross Linked Composites

3.1.1 Structure Description of MIL-53-NH_2

Chains of corner-sharing Al (III) octahedra coupled by 2-OH and carboxylate groups make up the MIL-53-NH_2 framework (Fig. 1a, inset). The amino terephthalate ions link these chains together to create a channel system with a 1D rhombohedral shape. These chains can be combined to create three different 3D frameworks. The tunnels (7.3 × 7.7 mm) in the parent MIL-53 was constructed from Al ions as nodes and benzene dicarboxylate molecules as linkers.

For XRD spectra, MIL-53-NH_2 show diffraction peaks at $2\theta^\circ = 8.8^\circ$, 10.4°, 12.4°, 15.1°, 17.63° and 26.5° (Fig. 1a). From XRD, the prepared material was well crystalline and in pure phase. The BET surface area for the prepared framework was 940 $m^2\ g^{-1}$.

The chemical group of MIL-53-NH_2 was monitored by FTIR. The O–H stretching vibrations located at 3375 cm^{-1}, the carboxylic group in the back bone of MIL-53-NH_2 solids were located at 1600 and 1505 cm^{-1}, which are attributed to an asymmetric stretching vibration (Fig. 1b). The band located around 485 cm^{-1} is associated to the Al-O stretching vibrational frequency. The SEM image of MIL-53-NH_2 shows the homogeneity in morphology and small hexagonally in shape with 0.2–0.5 µm diameter in size (Fig. 1c). The TEM of MIL-53-NH_2 is located in Fig. 1d, it is showed spherical shape with about 50 nm in size.

3.1.2 Structure Description of MOFCE24 Composite

Figure 2a shows the FTIR spectra of MIL-53-NH_2, dibenzo 24-crown-8 ether and MIL-53-NH_2-dibenzo-24-crown-8 ether composite. The FTIR spectrum of MOFCE24 ether composite is in strong agreement with the pure MIL-53-NH_2. Both MIL-53-NH_2 and MOFCE24 composite show absorption bands around 3375 cm^{-1} correspond to the O–H stretching vibrations. Two sharp bands centered at 1620 and 1426 cm^{-1} are assigned to the asymmetric and symmetric (COO^-) stretching vibrations respectively of terephthalate ion. The band located around 485 cm^{-1} is associated to the Al-O stretching vibrational frequency. Figure 2b displays the SEM image of dibenzo-24-crown-8 ether composite.

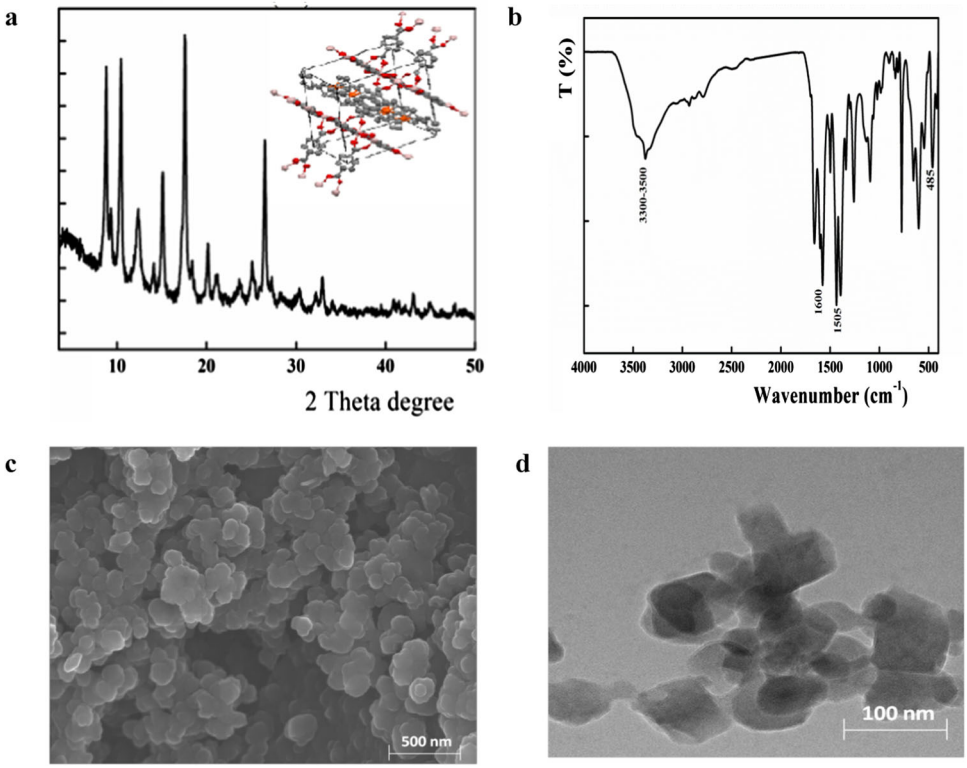

Fig. 1 XRD, FTIR, SEM and TEM of the parent MIL-53-NH_2 framework

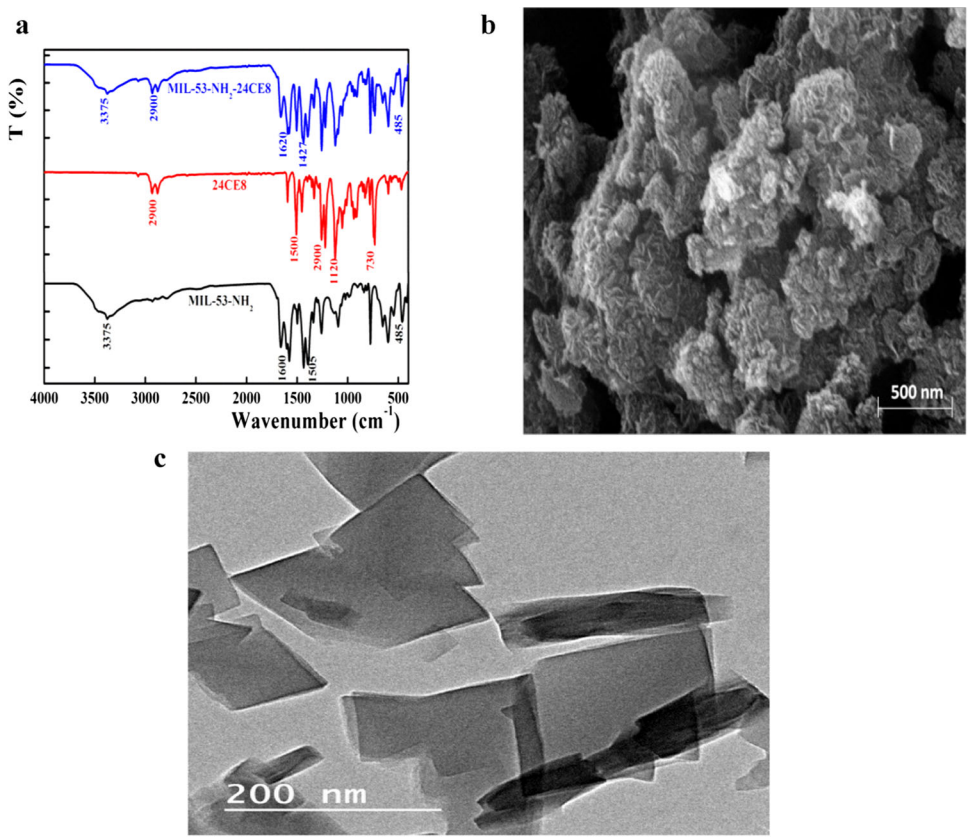

Fig. 2 FTIR, SEM and TEM of MOFCE24 composite

The image presented in Fig. 2c shows several flakes aggregated together of 24-dibenzo-8-ether@MIL-53-NH_2 particles with an average size between 200 and 300 nm indicating the effect of dibenzo-24-crown ether macromolecule in the MIL-53-NH_2 morphology, it is converted the spherical morphology of pure MIL-53-NH_2 to flakes shape of MOFCE24 particles.

3.1.3 Structure Description of MOFCE6 Composite

The FTIR spectra MIL-53-NH_2 and MOFCE6 composite (Figure S1) confirms the presence of free amine groups in the functionalized MOF. Absorption bands at 3497 cm^{-1}, which charged to the asymmetrical and symmetrical stretching vibration of amino group were recorded. Another absorption bands at 1335, 3631 and 3617 cm^{-1} are attributed to C-N stretching and bridging hydroxyl groups (Al–OH-Al), respectively.

SEM and TEM micrographs of MIL-53-NH_2 and MIL-53-NH_2–crown ether composite (Figure S1) showed homogeneous morphologies of both samples, except MIL-53-NH_2–crown ether composite particles are easier to identify because of their round shape compared with MIL-53-NH_2. According to figure S1c, the average particle size of MOFCE6 is 83 ± 13 nm. This clearly demonstrated an easy method for fabricating MOFs with controllable size and morphology.

3.1.4 Structure Description of MOFCalix Composite

In order to confirm the composite calixarene-MIL-53-NH_2 structure, the variations spectrum of IR was recorded (**S2**). The absorption peaks of the samples can provide enough information on the chemical structure transformation. Calixarene showed peak at 2960 cm^{-1} corresponds to the antisymmetric vibration of methylene groups. There was a peak at 778 cm^{-1}, possibly caused by the bending vibration of C-H in the benzene ring. The peak at 1440 cm^{-1} was attributed to the C = C double bond vibration in the benzene ring. MIL-53-NH_2 showed characteristic bands as illustrated before, the composite showed bands at 1402 cm^{-1} and 1607 cm^{-1} related to the symmetric and asymmetric stretching of the –COO in carboxyl group of organic ligand. Also, it showed the most bands of calixarene, for example, it showed the stretching vibration of –OH at 3249 cm^{-1}.

Figure S2b shows SEM images of MOFCalix. At lower magnification, the SEM images show that the samples consist of irregular clumps. The TEM image (Fig. 2Sc) shows that the blocks consist of flat objects stacked piece by piece.

3.2 Voltammetric Behavior of Lead at Macromolecules Modified Sensors

It is well known that lead ions are able to form metallic complexes with different macrocyclic compounds including crown ethers and calixarene [49–52]. Therefore, the electrochemical behavior of lead ions was explored on the bare screen-printed carbon sensors and those integrated with different macrocyclic compounds in acetate buffer solution (Fig. 3a). At the unmodified carbon electrodes, lead ion showed a broad oxidation peak at − 0.660 V with a limited peak current. Upon modification of the electrode surface with crown ethers or calixarene, a noticeable shifting of the peak potential toward more negative potential with improved peak performance was recorded, which can be explained on the basis of complexation with lead ions with the sensing element. Among the tested macromolecules, calixarene exhibited the proper performance as indicated by the highest peak current.

Next, the functionalized cross-linked metal–organic framework-macromolecules nanocomposites were tested as electrode modifier (Fig. 3b). Improvement of the peak height by about threefolds compared with the bare electrode and shifting of the peak potential by about 100 mV was the most promising futures of the tested cross-linked macromolecules. Among the different tested composites, both the MOFCE24 and MOFCalix were selected.

Compared with cyclic voltammetry, differential pulse voltammetric technique (DPV) offers the advantage of improved peak current with better resolution between the oxidation peaks for advanced selectivity of the analysis protocol. Herein, differential pulse voltammograms were used for simultaneous determination of Pb, Cd and Cu ions applying the selected electrode modifiers MOFCE24 and MOFCalix composites in acetate buffer solution pH 5.5 (Fig. 3c,d). While MOFCE24 showed improved oxidation current and more reproducible peaks for Pb and Cu ions, the oxidation peak for Cd was lower than that for MOFCalix. From the above results, we can conclude that MIL-53-NH_2-dibenzo 24-crown-8-ether appeared to be the most appropriate sensing element and will be selected for the next measurements.

Reduced graphene nanosheets were added to the MIL-53-NH_2-dibenzo 24-crown-8-ether solution forming a ternary composite (MIL-53-NH_2-dibenzo 24-crown-8-ether-rGO) as a trial to enhance the electroactive surface area and the electrode sensitivity. Unexpectedly, formation of such ternary nanocomposite did not improve the electrode performance, which may be explained on the basis of blocking of the complexation active sites in the MOFCE24 composite with reduced graphene nanosheets.

The electrochemical future of sensors modified with MOFCE24 was monitored in ferricyanide (FCN) solution

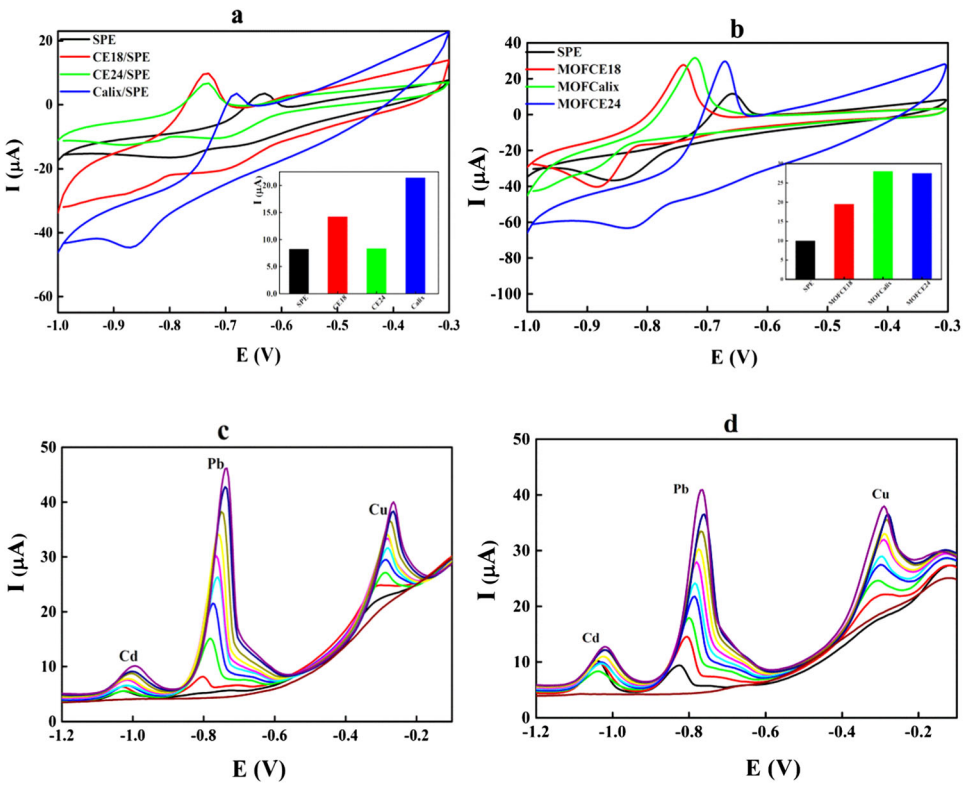

Fig. 3 Cyclic voltammograms recorded for 1.3 ppm Pb^{2+} in 2×10^{-1} mol L^{-1} acetate buffer pH 5.5 applying sensors dropcasted with; **a** free macromolecules; **b** *MIL-53-NH*$_2$-cross-linked macromolecules composites; **c**, **d** simultaneous DPV determination of Cd, Pb and Cu applying sensors dropcasted with MOFCE24 and MOFCalix

as the standard redox probe. The recorded cyclic voltammograms showed significant improvement of the faradaic current readouts accompanied with shifting of the peak potential as evidence to the existence catalytic functions of the nanocomposite (Figure S3). The electroactive surface area (EASA) of the modified electrodes was estimated through recording successive cyclic voltammograms in FCN solution at different scan rate values following the Randles—Sevik equation [53]. Sensors integrated with MIL-53-NH_2-dibenzo 24-crown-8-ether showed improved electroactive areas of 0.102 cm^2 compared with 0.071cm^2 recorded for the blank electrodes.

3.3 Effect of the Supporting Electrolytes

To attain the highest sensitivity of the method, DPVs were recorded using sensors integrated with MOFCE24 in different supporting electrolytes covering a wide pH range.

In acetate buffer medium, a noticeable gradual enhancement of the peak performance upon increasing the pH value was recorded with a maximum peak current at pH 5 (Fig. 4a). The peak potential was shifted toward the negative direction at elevated pH values postulating the participation of the proton in the electrode reaction takes place at the electrode surface [54]. This may be explained on the bases of the presence of some functional groups in the sensing elements (MOF or crown ethers), which are pH dependent. In the BR universal buffer, only a sharp and reproducible peak was recorded at pH 2 with an oxidation potential of − 0.64 V (Fig. 4b).

Moreover, the electrochemical behavior of the constructed sensor was explored in different supporting electrolytes including KCl, HCl or HNO_3 (Fig. 4c). Among the tested supporting electrolytes, both HCl and acetate buffer were the most proper. Even though HCl medium exhibited higher peak current compared to acetate buffer (about two folds), the simultaneous determination of Cd, Pb and Cu was allowed only in acetate buffer medium (Fig. 4d).

3.4 Effect of the Scan Rate

Performing cyclic voltammograms at different scan rates provides a detailed explanation about the oxidation mechanism of the target analyte and the number of electrons that participate in the oxidation process [54]. Herein, the effect of the scan rate was carried out utilizing both the bare electrodes and those integrated with MOFCE24 in HCl media (Fig. 5 and Figure S4). Improving of the peak height with noticeable shifting of the peak potential toward more positive was observed demonstrating the irreversibility of the electrode reaction (Fig. 5a, Figure S 4a). The peak heights were improved linearly ($r = 0.9973$) against the scan rate as illustrated in Fig. 5b sustaining the irreversibility process.

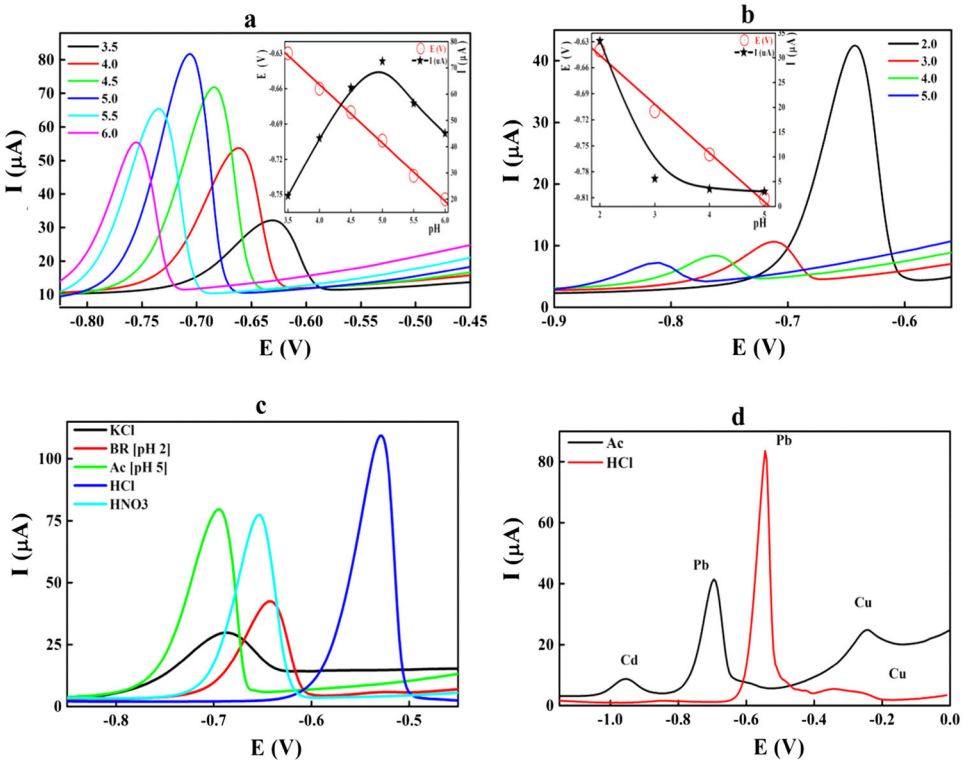

Fig. 4 Differential pulse voltammograms recorded for 3.0 ppm lead at MOFCE24-based sensors, **a** in acetate buffer solution, **b** universal buffer, **c** different supporting electrolyte and **d** simultaneous DPV determination of Cd, Pb and Cu in acetate and HCl supporting electrolytes

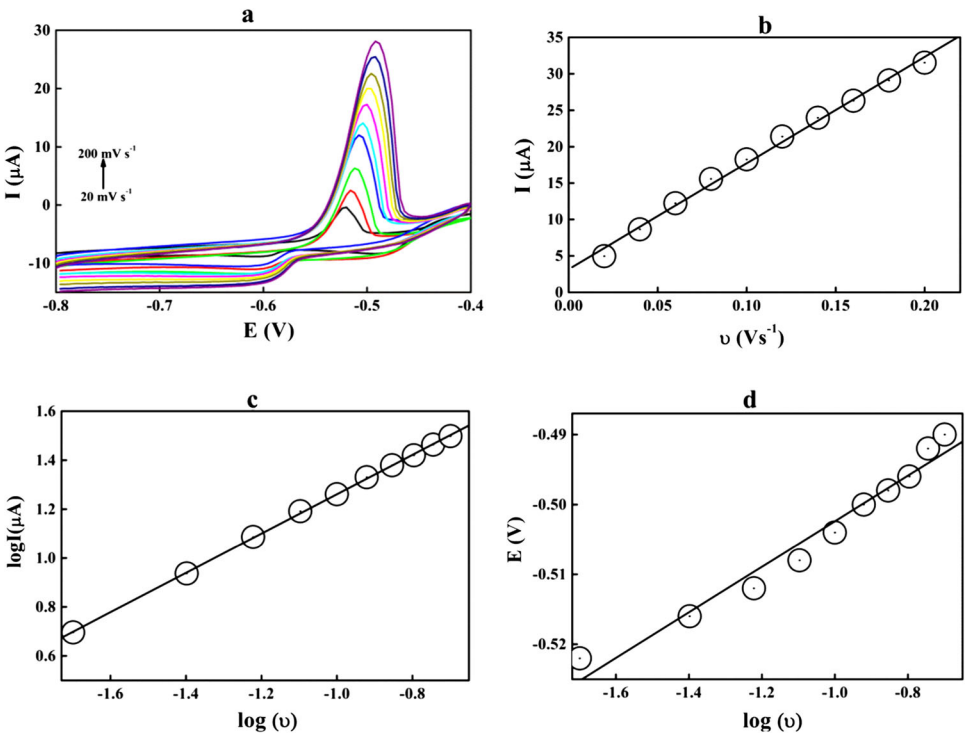

Fig. 5 Cyclic voltammograms for 4.0 ppm lead at MOFCE24 in HCl media recorded at different sweep rates, **b** peak current against the scan rate, **c** logarithmic value of the peak current against logarithmic value of the scan rate and **d** peak potential against logarithmic value of the scan rate

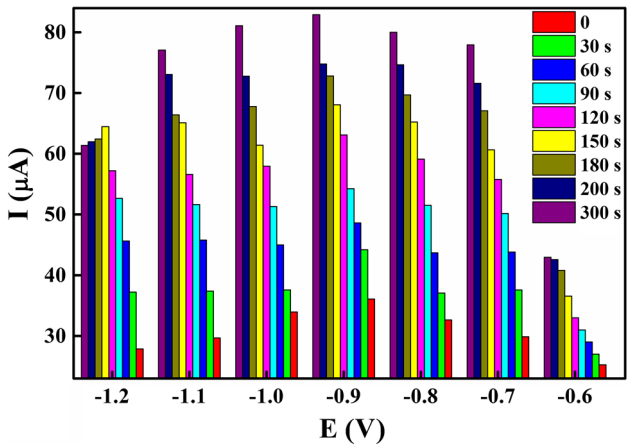

Fig. 6 Influence of the deposition potential and time on the peak current of 3.0 ppm lead at MOFCE24-based sensor in HCl medium

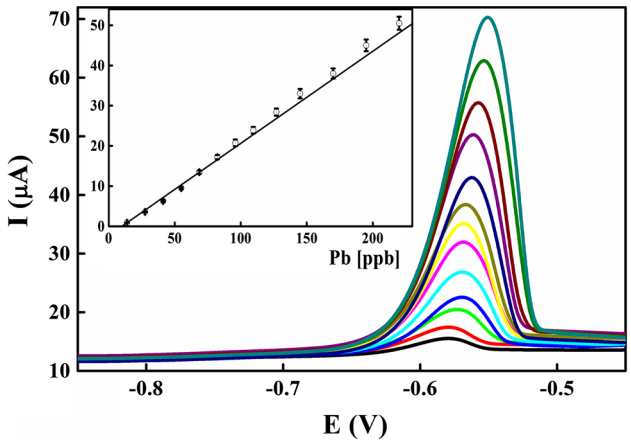

Fig. 7 Adsorptive differential pulse voltammetric determination of lead in 0.2 M HCl solution at MOFCE24 integrated sensors. Scan rate value was 0.050 Vs^{-1}, accumulation potential was − 0.9 V and accumulation time 300 s

Moreover, the logarithmic values of the peak current were correlated linearly with the logarithm value of the corresponding scan rate (Fig. 5c) with slope values of 0.9998, respectively, sustaining the pure adsorption controlled reaction mechanism [55, 56]. Lower slope value (0.8550, Figure S4c) was estimated in the case of bare screen printed sensors, which may be attributed to the electrocatalytic effect of the synthesized nanocomposite.

Finally, the peak potential recorded at different sweep rates showed linear relationship against logarithmic value of the sweep rate (Fig. 5d and figure S4d) with slope values 0.0325, suggesting the participation of two electrons in the electrode reaction according to Laviron equation [57].

Based on the scan rate results, it is clear that the electrode reaction mechanism was assumed to be an adsorption-controlled reaction; therefore, the influence of both accumulation time and deposition potential on the lead peak height was examined (Fig. 6). The recorded peak current increased with the deposition potential to reach its maximum value at − 0.9 V for 300 s accumulation time.

3.5 Linearity of the Method

Applying the optimized electroanalytical conditions, the performance characteristics of the introduced lead disposable sensors integrated with MIL-53-NH_2-dibenzo 24-crown-8-ether nanocomposite were evaluated. Different increments of the lead stock solution were added to the measuring cell and the corresponding peak currents were illustrated against the concentration of lead ion (Fig. 7 and Table 1). Calibration curves were linear within the lead concentration ranged from 13.75 to 217.83 ppb with high correlation coefficient (r = 0.9978). The limit of detection (LOD) and quantification (LOQ) were estimated according to the official methods [58], where LOQ equal to 10 × (SD/S) and LOD 3.3 × (SD/S). SD is the standard deviation of the intercept and S is the slope of the calibration curves. The estimated LOD and LOQ values were 3.18 and 9.62 ppb, respectively.

Table 1 Adsorptive differential pulse voltammetric determination of lead at MOFCE24-based sensors

Parameters	
Linearity rang (ppb)	13.75–217.83
Intercept (μA cm^{-2})	− 5.34
SD of intercept(μA cm^{-2})	0.27
Slope (μA mL^{-1} ng^{-1})	0.28
SD of slope (μA mL^{-1} ng^{-1})	0.01
Multiple *R*	0.9978
R Square	0.9956
RSD %	1.16
LOD (ppb)	3.18
LOQ (ppb)	9.64
Reproducibility of the peak current (RSD %)	1.12
Repeatability of the peak current (RSD %)	0.72
Reproducibility of the peak potential (RSD %)	0.823
Repeatability of the peak potential (RSD %)	0.941

[a]Obtained from an average of three experiments

The fabricated sensors showed high measurement reproducibility of the peak current and peak potential. Even though the fabricated sensors are disposable; the same electrode can be used for more than 15 successive measurements without diminishing its performance of the peak height (average recovery 100 ± 1.09%, Figure S5). Moreover, the fabrication reproducibility was performed through drop-casting of

Table 2 Determination of lead in water samples and biological fluids

Sample	Added (ng mL^{-1})	Found (ng mL^{-1})	Recovery* (%)	Reference method
Tap water	28.00	28.26 ± 0.46	100.93 ± 1.75	27.66 ± 0.82
River Nile water	16.00	16.66 ± 0.12	104.13 ± 075	15.24 ± 0.42
Human Blood	55.00	55.17 ± 0.62	100.31 ± 1.12	56.72 ± 1.06
Human Urine	11.00	11.06 ± 0.65	100.54 ± 5.91	10.55 ± 1.22

* Average of three replicates

five disposable sensors with 2 successive of 10 μL aliquots of the MOFCE24 nanocomposite suspension in DMF. DPVs recorded for 100 ppb of lead estimated an average peak height of 37.5 ± 0.85 μA showing the high reproducibility of the fabrication protocol. The stability of the fabricated sensors was evaluated over long storage period through recording of the voltammograms for a fixed lead concentration. Within the first month, the peak height remains constant (95.0% of the primary peak heights) and diminished to about 89.2% after 60 days of contentious operation (Figure S5). The prolonged operational lifetime represents one of the most promising futures of the cross-linked ionophore with limited leaching of the sensing element into the measuring solution [59].

Moreover, calibration curves for lead ions were performed by applying different electroanalytical detection techniques including cyclic voltammetry (CV), differential pulse voltammetry (DPV) and square wave voltammetry (SWV). Cyclic voltammetric measurements revealed lower peak current values compared with DPV and SWV. Both SWV and DPV showed approximately similar sensitivities with more reproducible and stable oxidation peaks recorded for DPV (Figure S5).

Finally, the performance of the newly fabricated screen-printed sensors integrated with MOFCE24 nanocomposite as sensing elements was compared with some previously reported lead sensors (Table S1). Improved sensitivity with prolonged operational and shelf lifetime were the most promising future of the introduced sensors with the diversity of analyzed samples. Moreover, the synergistic effect of the metal–organic frameworks as transducer and dibenzo 24-crown-8-ether as sensing elements accelerate the electron transfer process at the electrode surface and improve the sensor selectivity through complexation of the lead ions with the crown ether moiety.

3.6 Sample Analysis

The fabricated lead disposable screen-printed sensors integrated with MOFCE24 nanostructure showed improved selectivity and sensitivity toward Pb^{2+}; therefore, their applicability for quantification of lead in the environmental and biological samples was evaluated. The lead content was assayed voltammetrically following the optimized analysis protocol compared to the official spectroscopic method. The achieved high recoveries with lower relative standard deviation values encourage the applicability of the proposed analysis protocol (Table 2). Moreover, the introduced instrumentation protocol is suitable for the onsite measurement of lead in environmental samples without the requirements of transferring the analyzed sample to central laboratories.

4 Conclusion

The present work deals with synthesis and characterization of novel functionalized metal–organic framework cross-linked with dibenzo 24-crown-8-ether for sensitive and selective differential pulse voltammetric determination of lead in environmental samples and biological fluids. The synthesized nanocomposite showed the proper electrocatalytic activity toward lead ions through synergistic effect of the crown ether moiety through complexation with lead ions and the nanostructured metal–organic framework as transducer, which accelerate the electron transfer process at the electrode surface. The cited sensors showed improved sensitivity within the lead concentration ranging from 13.75 to 217.83 ppb with LOD and LOQ values of 3.18 and 9.62 ppb, respectively. The constructed disposable sensors showed high measuring reproducibility and long operational life time (60 days) based on formation of cross-linked ionophore/metal–organic framework. The fabricated sensors can be introduced as an efficient tool for sensitive and reliable onsite voltammetric determination of lead in environmental and biological sample with acceptable average recoveries comparable with the official method.

Supplementary Information The online version contains supplementary material available at https://doi.org/10.1007/s13369-023-08267-w.

Acknowledgements The authors express their great gratitude to the project fund received from the National Research Centre (NRC, Cairo, Egypt) for the internal grant (No. 1210406).

Funding Open access funding provided by The Science, Technology & Innovation Funding Authority (STDF) in cooperation with The Egyptian Knowledge Bank (EKB).

Availability of Data and Materials All data generated or analyzed during this study are included in this published article and its supplementary information files.

Declarations

Conflict of interest The authors declare that they have no conflict of interests.

References

1. Baghayeri, M.; Amiri, A.; Moghaddam, B.S.; Nodehi, M.: Cu-Based MOF for simultaneous determination of trace Tl (I) and Hg (II) by stripping voltammetry. J. Electrochem. Soc. **167**(16), 167522 (2020)
2. Ghanei-Motlagh, M.; Baghayeri, M.: Application of N, S-dual-doped carbon/sepiolite clay hybrid material for electrochemical detection of mercury (II) in water resources. Mater. Chem. Phys. **285**, 126127 (2022)
3. Baghayeri, M.; Amiri, A.; Karimabadi, F.; Di Masi, S.; Maleki, B.; Adibian, F.; Pourali, A.R.; Malitesta, C.: Magnetic MWCNTs-dendrimer: a potential modifier for electrochemical evaluation of As (III) ions in real water samples. J. Electroanal. Chem. **888**, 115059 (2021)
4. Rodriguez, B.B.; Bolbot, J.A.; Tothill, I.E.: Urease–glutamic dehydrogenase biosensor for screening heavy metals in water and soil samples. Anal. Bioanal. Chem. **380**, 284–292 (2004)
5. Rodriguez, B.B.; Bolbot, J.A.; Tothill, I.E.: Development of urease and glutamic dehydrogenase amperometric assay for heavy metals screening in polluted samples. Biosens. Bioelectron. **19**(10), 1157–1167 (2004)
6. Al-Saleh, I.A.: The biochemical and clinical consequences of lead poisoning. Med. Res. Rev. **14**(4), 415–486 (1994)
7. Bressler, J.; Kim, K.A.; Chakraborti, T.; Goldstein, G.: Molecular mechanisms of lead neurotoxicity. Neurochem. Res. **24**, 595–600 (1999)
8. Fitch, A.: Lead analysis: past and present. Crit. Rev. Anal. Chem. **28**(3), 267–345 (1998)
9. Liu, H.; Baghayeri, M.; Amiri, A.; Karimabadi, F.; Nodehi, M.; Fayazi, M.; Maleki, B.; Zare, E.N.; and Kaffash, A.: A strategy for As (III) determination based on ultrafine gold nanoparticles decorated on magnetic graphene oxide. Environ. Res. 116177 (2023)
10. Nodehi, M.; Baghayeri, M.; Kaffash, A.: Application of BiNPs / MWCNTs-PDA / GC sensor to measurement of Tl (1) and Pb (II) using stripping voltammetry. Chemosphere **301**, 134701 (2022)
11. Koshki, M.S.; Baghayeri, M.; Fayazi, M.: Application of sepiolite/FeS2 nanocomposite for highly selective detection of mercury (II) based on stripping voltammetric analysis. J. Food Meas. Charact. **15**(6), 5318–5325 (2021)
12. Radu, A.; Radu, T.; Mc Graw, C.; Dillingham, P.; Anastasova-Ivanova, S.; Diamond, D.: Ion selective electrodes in environmental analysis. J. Serb. Chem. Soc. **78**(11), 1729–1761 (2013)
13. Kalcher, K.; Švancara, I.; Metelka, R.; Vytřas, K.; Walcarius, A.: Heterogeneous carbon electrochemical sensors. Encycl. Sens. **4**, 283 (2006)
14. Yantasee, W.; Lin, Y.; Hongsirikarn, K.; Fryxell, G.E.; Addleman, R.; Timchalk, C.: Electrochemical sensors for the detection of lead and other toxic heavy metals: the next generation of personal exposure biomonitors. Environ. Health Perspect. **115**(12), 1683–1690 (2007)
15. Kang, W.; Pei, X.; Rusinek, C.A.; Bange, A.; Haynes, E.N.; Heineman, W.R.; Papautsky, I.: Determination of lead with a copper-based electrochemical sensor. Anal. Chem. **89**(6), 3345–3352 (2017)
16. Raril, C.; Manjunatha, J.G.: Fabrication of novel polymer-modified graphene-based electrochemical sensor for the determination of mercury and lead ions in water and biological samples. J. Anal. Sci. Technol. **11**(1), 1 (2020)
17. Bahrami, A.; Besharati-Seidani, A.; Abbaspour, A.; Shamsipur, M.: A highly selective voltammetric sensor for sub-nanomolar detection of lead ions using a carbon paste electrode impregnated with novel ion imprinted polymeric nanobeads. Electrochim. Acta **118**, 92–99 (2014)
18. Silva, R.R.; Raymundo-Pereira, P.A.; Campos, A.M.; Wilson, D.; Otoni, C.G.; Barud, H.S.; Costa, C.A.; Domeneguetti, R.R.; Balogh, D.T.; Ribeiro, S.J.; Oliveira, O.N., Jr.: Microbial nanocellulose adherent to human skin used in electrochemical sensors to detect metal ions and biomarkers in sweat. Talanta **218**, 121153 (2020)
19. De Campos, A.M.; Silva, R.R.; Calegaro, M.L.; Raymundo-Pereira, P.A.: Design and fabrication of flexible copper sensor decorated with bismuth micro / nanodentrites to detect lead and cadmium in noninvasive samples of sweat. Chemosensors **10**(11), 446 (2022)
20. Wang, Y.; Liu, Z.; Hu, X.; Cao, J.; Wang, F.; Xu, Q.; Yang, C.: On-line coupling of sequential injection lab-on-valve to differential pulse anodic stripping voltammetry for determination of Pb in water samples. Talanta **77**(3), 1203–1207 (2009)
21. Vieira dos Santos, A.C.; Masini, J.C.: Development of a sequential injection anodic stripping voltammetry (SI-ASV) method for determination of Cd (II), Pb (II) and Cu (II) in wastewater samples from coatings industry. Anal. Bioanal. Chem. **385**, 1538–1544 (2006)
22. Siriangkhawut, W.; Grudpan, K.; Jakmunee, J.: Sequential injection anodic stripping voltammetry with monosegmented flow and in-line UV digestion for determination of Zn (II), Cd (II), Pb (II) and Cu (II) in water samples. Talanta **84**(5), 1366–1373 (2011)
23. Wang, J.; Lu, J.; Hocevar, S.B.; Farias, P.A.; Ogorevc, B.: Bismuth-coated carbon electrodes for anodic stripping voltammetry. Anal. Chem. **72**(14), 3218–3222 (2000)
24. Economou, A.: Bismuth-film electrodes: recent developments and potentialities for electroanalysis. TrAC, Trends Anal. Chem. **24**(4), 334–340 (2005)
25. Thanh, N.M.; Luyen, N.D.; Thanh Tam Toan, T.; Hai Phong, N.; Van Hop, N.: Voltammetry determination of Pb (II), Cd (II), and Zn (II) at bismuth film electrode combined with 8-hydroxyquinoline as a complexing agent. J. Anal. Methods Chem. (2019)
26. Cox, J.A.; Tess, M.E.; Cummings, T.E.: Electroanalytical methods based on modified electrodes: a review of recent advances. Rev. Anal. Chem. **15**(3), 173–224 (1996)
27. Khaled, E.; Hassan, H.N.A.; Habib, I.H.I.; Metelka, R.: Chitosan modified screen-printed carbon electrode for sensitive analysis of heavy metals. Int. J. Electrochem. Sci. **5**(2), 158–167 (2010)
28. Xia, G.; Zheng, Y.; Sun, Z.; Xia, S.; Ni, Z.; Yao, J.: Fabrication of ZnAl-LDH mixed metal-oxide composites for photocatalytic

degradation of 4-chlorophenol. Environ. Sci. Pollut. Res. **29**(26), 39441–39450 (2022)
29. Ma, Y.; Leng, Y.; Huo, D.; Zhao, D.; Zheng, J.; Yang, H.; Zhao, P.; Li, F.; Hou, C.: A sensitive enzyme-free electrochemical sensor based on a rod-shaped bimetallic MOF anchored on graphene oxide nanosheets for determination of glucose in huangshui. Anal. Methods (2023)
30. Zhang, W.; Ma, H.; Li, T.; He, C.: Rational design of a novel two-dimensional porous metal-organic framework material for efficient benzene sensor. Chin. Chem. Lett. **33**(8), 3726–3732 (2022)
31. Karimi-Maleh, H.; Liu, Y.; Li, Z.; Darabi, R.; Orooji, Y.; Karaman, C.; Karimi, F.; Baghayeri, M.; Rouhi, J.; Fu, L.; Rostamnia, S.: Calf thymus ds-DNA intercalation with pendimethalin herbicide at the surface of ZIF-8/Co/rGO/C3N4/ds-DNA/SPCE: a bio-sensing approach for pendimethalin quantification confirmed by molecular docking study. Chemosphere **332**, 138815 (2023)
32. Karimi-Maleh, H.; Darabi, R.; Karimi, F.; Karaman, C.; Shahidi, S.A.; Zare, N.; Baghayeri, M.; Fu, L.; Rostamnia, S.; Rouhi, J.; Rajendran, S.: State-of-art advances on removal, degradation and electrochemical monitoring of 4-aminophenol pollutants in real samples: a review. Environ. Res. 115338 (2023)
33. Liu, W.; Yin, X.B.: Metal–organic frameworks for electrochemical applications. TrAC Trends Anal. Chem. **75**, 86–96 (2016)
34. Li, W.J.; Tu, M.; Cao, R.; Fischer, R.A.: Metal–organic framework thin films: electrochemical fabrication techniques and corresponding applications & perspectives. J. Mater. Chem. A **4**(32), 12356–12369 (2016)
35. Xu, Y.; Li, Q.; Xue, H.; Pang, H.: Metal-organic frameworks for direct electrochemical applications. Coord. Chem. Rev. **376**, 292–318 (2018)
36. Liu, L.; Zhou, Y.; Liu, S.; Xu, M.: The applications of metal− organic frameworks in electrochemical sensors. Chem. Electro Chem. **5**(1), 6–19 (2018)
37. Fang, X.; Zong, B.; Mao, S.: Metal–organic framework-based sensors for environmental contaminant sensing. Nano-micro Lett. **10**, 1–19 (2018)
38. Wang, Y.; Wu, Y.; Xie, J.; Hu, X.: Metal–organic framework modified carbon paste electrode for lead sensor. Sens. Actuators B Chem. **177**, 1161–1166 (2013)
39. Guo, H.; Wang, D.; Chen, J.; Weng, W.; Huang, M.; Zheng, Z.: Simple fabrication of flake-like NH2-MIL-53 (Cr) and its application as an electrochemical sensor for the detection of Pb2+. Chem. Eng. J. **289**, 479–485 (2016)
40. Guo, H.; Zheng, Z.; Zhang, Y.; Lin, H.; Xu, Q.: Highly selective detection of Pb2+ by a nanoscale Ni-based metal–organic framework fabricated through one-pot hydrothermal reaction. Sens. Actuators, B Chem. **248**, 430–436 (2017)
41. Lu, M.; Deng, Y.; Luo, Y.; Lv, J.; Li; T.; Xu, J.; Chen, S.W.; Wang, J.: Graphene aerogel–metal–organic framework-based electrochemical method for simultaneous detection of multiple heavy-metal ions. Anal. Chem. **91** (1), 888–895 (2018)
42. Hu, Z.; Xu, Y.; Wang, H.; Fan, G.C.; Luo, X.: Self-powered anti-interference photoelectrochemical immunosensor based on Au/ZIS/CIS heterojunction photocathode with zwitterionic peptide anchoring. Chin. Chem. Lett. **33**(11), 4750–4755 (2022)
43. Huang, K.; Xu, Q.; Ying, Q.; Gu, B.; Yuan, W.: Wireless strain sensing using carbon nanotube composite film. Compos. B Eng. **256**, 110650 (2023)
44. Xia, H.; Zan, L.; Yuan, P.; Qu, G.; Dong, H.; Wei, Y.; Yu, Y.; Wei, Z.; Yan, W.; Hu, J.S.; Deng, D.: Evolution of stabilized 1T-MoS2 by atomic-interface engineering of 2H-MoS2/Fe− Nx towards enhanced sodium ion storage. Angew. Chem. **135**(14), e202218282 (2023)
45. Wang, Z.; Fu, W.; Hu, L.; Zhao, M.; Guo, T.; Hrynsphan, D.; Tatsiana, S.; Chen, J.: Improvement of electron transfer efficiency during denitrification process by Fe-Pd/multi-walled carbon nanotubes: Possessed redox characteristics and secreted endogenous electron mediator. Sci. Total Environ. **781**, 146686 (2021)
46. Saeed, R.; Feng, H.; Wang, X.; Zhang, X.; Fu, Z.: Fish quality evaluation by sensor and machine learning: a mechanistic review. Food Control **137**, 108902 (2022)
47. Mahajan, R.K.; Walia, T.P.; Kaur, S.: Stripping voltammetric determination of zinc, cadmium, lead and copper in blood samples of children aged between 3 months and 6 years. Online J. Health Allied Sci. **4** (1) (2005)
48. Hassan, R.Y.; Habib, I.H.; Hassan, H.N.: Voltammetric determination of lead (II) in medical lotion and biological samples using chitosan-carbon paste electrode. Int. J. Electrochem. Sci. **3**(8), 935–945 (2008)
49. Khaled, E.; Kamel, M.S.; Hassan, H.N.A.: Novel multi walled carbon nanotubes/crown ether based disposable sensors for determination of lead in water samples. Anal. Chem. Lett. **5**(6), 329–337 (2015)
50. Shamsipur, M.; Ganjali, M.R.; Rouhollahi, A.: Lead-selective membrane potentiometric sensor based on an 18-membered thiacrown derivative. Anal. Sci. **17**(8), 935–938 (2001)
51. Yaftian, M.R.; Rayati, S.; Emadi, D.; Matt, D.: A coated wire-type lead (II) ion-selective electrode based on a phosphorylated calix [4] arene derivative. Anal. Sci. **22**(8), 1075–1078 (2006)
52. Isvoranu, M.; Luca, C.; Pleniceanu, M.; Spinu, C.: Studies on a Pb2+-selective electrode with a macrocyclic liquid membrane: Potentiometric determination of pb2+ ions. J. Serb. Chem. Soc. **71**(12), 1345–1352 (2006)
53. Stanković, D.; Mehmeti, E.; Svorc, L.; Kalcher, K.: New electrochemical method for the determination of β-carboline alkaloids, harmalol and harmine, in human urine samples and in Banisteriopsis caapi. Microchem. J. **118**, 95–100 (2015)
54. Zhang, Z.; Wang, E.: Electrochemical Principles and Methods. Science Press, Beijing (2000)
55. Gosser, D.K.: Cyclic voltammetry: simulation and analysis of reaction mechanisms (Vol. 43). New York: VCH (1993)
56. Elgrishi, N.; Rountree, K.J.; McCarthy, B.D.; Rountree, E.S.; Eisenhart, T.T.; Dempsey, J.L.: A practical beginner's guide to cyclic voltammetry. J. Chem. Educ. **95**(2), 197–206 (2018)
57. Laviron, E.: Theoretical study of a reversible reaction followed by a chemical reaction in thin layer linear potential sweep voltammetry. J. Electroanal. Chem. Interfacial Electrochem. **39**(1), 1–23 (1972)
58. Currie, L.A.: International Recommendations Offered on Analytical Detection and Quantification Concepts and Nomenclature: Preamble, in Validation of Analytical Methods (1999)
59. Khaled, E.; Kamel, M.S.; Hassan, H.N.; Haroun, A.A.; Youssef, A.M.; Aboul-Enein, H.Y.: Novel multi walled carbon nanotubes/β-cyclodextrin based carbon paste electrode for flow injection potentiometric determination of piroxicam. Talanta **97**, 96–102 (2012)